Published OnlineFirst September 1, 2020; DOI: 10.1158/0008-5472.CAN-20-2002

Phosphorylation Control of p53 DNA-Binding Cooperativity Balances Tumorigenesis and Aging

Oleg Timofeev[1], Lukas Koch[1], Constantin Niederau[1], Alina Tscherne[1], Jean Schneikert[1], Maria Klimovich[1], Sabrina Elmshäuser[1], Marie Zeitlinger[1], Marco Mernberger[1], Andrea Nist[2], Christian Osterburg[3], Volker Dötsch[3], German Mouse Clinic Consortium, Martin Hrabé de Angelis[4,5,6], and Thorsten Stiewe[1,2]

ABSTRACT

Posttranslational modifications are essential for regulating the transcription factor p53, which binds DNA in a highly cooperative manner to control expression of a plethora of tumor-suppressive programs. Here we show at the biochemical, cellular, and organismal level that the cooperative nature of DNA binding is reduced by phosphorylation of highly conserved serine residues (human S183/S185, mouse S180) in the DNA-binding domain. To explore the role of this inhibitory phosphorylation *in vivo*, new phosphorylation-deficient p53-S180A knock-in mice were generated. Chromatin immunoprecipitation sequencing and RNA sequencing studies of S180A knock-in cells demonstrated enhanced DNA binding and increased target gene expression. *In vivo*, this translated into a tissue-specific vulnerability of the bone marrow that caused depletion of hematopoietic stem cells and impaired proper regeneration of hematopoiesis after DNA damage. Median lifespan was significantly reduced by 20% from 709 days in wild type to only 568 days in S180A littermates. Importantly, lifespan was reduced by a loss of general fitness and increased susceptibility to age-related diseases, not by increased cancer incidence as often seen in other p53-mutant mouse models. For example, S180A knock-in mice showed markedly reduced spontaneous tumorigenesis and increased resistance to *Myc*-driven lymphoma and *Eml4–Alk*-driven lung cancer. Preventing phosphorylation of S183/S185 in human cells boosted p53 activity and allowed tumor cells to be killed more efficiently. Together, our data identify p53 DNA-binding domain phosphorylation as a druggable mechanism that balances tumorigenesis and aging.

Significance: These findings demonstrate that p53 tumor suppressor activity is reduced by DNA-binding domain phosphorylation to prevent aging and identify this phosphorylation as a potential target for cancer therapy.

See related commentary by Horikawa, p. 5164

Introduction

TP53 is arguably the most powerful tumor suppressor that governs a plethora of cellular programs, some of which can support survival and provide recovery of the cell after damage, whereas others lead to cell death. As a transcription factor, p53 controls expression of hundreds of genes, creating a sophisticated regulatory network that requires a tight regulation of p53 itself. Complex patterns of posttranslational modifications (PTM) under basal conditions or upon stress determine subcellular localization, transcriptional activity, and stability of the p53 protein (1). Multiple phosphorylation sites, involved in the regulation of p53′s stability, transcriptional activity, and nontranscriptional functions were identified in the N- and C-terminal domains (1). In addition, several important modifications, such as Lys^{120} and Lys^{164} acetylation, which enhance transactivation and induction of p53-dependent apoptosis, were mapped to the DNA-binding domain (DBD; refs. 2–4). The functional significance of other PTMs in the DBD is less well established. Phosphorylation of the DBD residues Ser^{183}, Thr^{211}, and Ser^{215} by Aurora B kinase was shown to promote p53 degradation via the ubiquitin-dependent proteasomal pathway (5). Similarly, Ser^{183}, Ser^{269}, and Thr^{284} were identified as Aurora B kinase phosphorylation sites that inhibit the transcriptional activity of p53 (6). Moreover, extensive mass spectrometry analyses confirmed these DBD phosphorylation sites and identified Ser^{185} as a novel site (7, 8). Whether and how these DBD phosphorylation events affect DNA binding remains unclear.

p53 binds DNA as a tetramer in a sequence-specific manner. Its prototypical response element (RE) consists of two decameric RRRCWWGYYY half-sites (where R = A, G; W = A, T; Y = C, T) separated by a facultative spacer of 1–21 bases (9). The binding by four monomers is cooperative and the degree of cooperativity determined by structural properties encoded in the RE base sequence (10, 11). p53 binds with high affinity and low cooperativity to REs with a central CATG sequence that possess a high torsional flexibility, whereas binding to more rigid CAAG, CTTG, and CTAG REs, frequently found in promoters of proapoptotic target genes, occurs with a high degree of cooperativity (9, 11, 12). DNA-binding cooperativity therefore differs within the p53 cistrome and distinguishes, for instance, p53′s proapoptotic and apoptosis-independent functions (13–16). Cooperative DNA binding is structurally not only supported by p53′s dedicated tetramerization domain, but also by interactions between neighboring DNA-binding core domains, in particular, by reciprocal

[1]Institute of Molecular Oncology, Member of the German Center for Lung Research (DZL), Philipps-University Marburg, Marburg, Germany. [2]Genomics Core Facility, Philipps-University Marburg, Marburg, Germany. [3]Institute of Biophysical Chemistry, Goethe University, Frankfurt, Germany. [4]German Mouse Clinic, Institute of Experimental Genetics, Helmholtz Zentrum München, German Research Center for Environmental Health, Neuherberg, Germany. [5]Chair of Experimental Genetics, School of Life Science Weihenstephan, Technische Universität München, Freising, Germany. [6]German Center for Diabetes Research (DZD), Neuherberg, Germany.

Note: Supplementary data for this article are available at Cancer Research Online (http://cancerres.aacrjournals.org/).

Consortium full list of authors and their affiliations is available in supplementary data at Cancer Research Online (http://cancerres.aacrjournals.org/).

M. Hrabé de Angelis and T. Stiewe contributed equally to this work.

Corresponding Authors: Thorsten Stiewe, Philipps-University Marburg, 35037 Marburg, Germany. Phone: 49-6421-28-26280; E-mail: stiewe@uni-marburg.de; and Oleg Timofeev, timofeev@staff.uni-marburg.de

Cancer Res 2020;80:5231–44

doi: 10.1158/0008-5472.CAN-20-2002

Published OnlineFirst September 1, 2020; DOI: 10.1158/0008-5472.CAN-20-2002

salt bridges formed by the oppositely charged amino acids Glu^{180} and Arg^{181} of the short H1 helix (17–20). A reduction in cooperativity dramatically affects sequence-specific DNA binding of p53 and disturbs its physiologic functions *in vivo* (13–16, 21). For example, the cooperativity-reducing mutation E180R leads to loss of binding to proapoptotic gene promoters, causing a selective defect in DNA damage–triggered apoptosis and compromised tumor suppression (15), whereas the R181E substitution has an even more pronounced effect on DNA binding and abolishes the transcriptional activity completely (14, 16). It is therefore not surprising that cooperativity-reducing Glu^{180} and Arg^{181} mutations form a mechanistically distinct class of tumor-associated p53 mutations found in an estimated number of 34,000 patients with cancer per year worldwide (16, 22).

The phosphorylation sites Ser^{183} (S183) and Ser^{185} (S185) are located in direct vicinity to the H1 helix salt bridge residues, tempting us to speculate that phosphorylation of these serine residues may affect DNA-binding cooperativity and represent a mechanism for controlling DNA binding–dependent p53 functions.

Materials and Methods

Animal experiments

The B6.129S/Sv-*Trp53*^{tm3Thst} knock-in mouse with the conditional *Trp53*$^{LSL\text{-}S180A}$ (TCC>GCC) mutation was generated by Ingenious Targeting Laboratory as described previously (15). *Trp53*$^{+/LSL\text{-}S180A}$ mice were crossed with 129S/Sv-Tg(Prm-cre)58Og/J animals to obtain *Trp53*$^{+/S180A}$ mice, which were intercrossed to generate homozygous animals and wild-type (WT) mice as littermate controls. *Trp53*$^{LSL\text{-}S180A/LSL\text{-}S180A}$ mice were used as p53-negative controls.

For generation of B-cell lymphoma, *Trp53*$^{+/S180A}$ females were crossed with B6.Cg-Tg(IghMyc)22Bri/J males (23). For somatic CRISPR-induced lung mutagenesis (24), we used age- and gender-matched *Trp53*$^{S180/S180A}$ and WT littermates carrying a floxed luciferase reporter [B6.129-*Gt(ROSA)26Sor*$^{tm2(ACTB\text{-}Luc)Tyj}$/Nci] to monitor lung tumorigenesis by bioluminescence imaging (BLI). Recombinant CRISPR-adenovirus [1×10^{10}–5×10^{10} PFU (plaque forming units)] was delivered intratracheally as described previously (25). Mouse imaging was performed using the In Vivo Xtreme II System (Brucker), 7T Clinscan 70/30 USR (Brucker) or CT nanoScan PET-CT (Mediso).

For studying acute DNA damage responses, mice were subjected to an X-ray dose of 6 Gy (1 Gy/minute) using an X-RAD 320iX (Precision X-Ray) irradiator. In muscle regeneration experiments, mice of both genders were used as described previously (26, 27).

A cohort of 57 littermates, 15 mutant males and 15 control males, 14 mutant females and 13 control females, were phenotypically analyzed at the German Mouse Clinic (GMC) at the age of 8 to 19 weeks. The standardized screening pipeline for systematic primary phenotyping was described previously (28). Mouse phenotyping methods were reported before (29–31).

All mouse experiments were performed according to the German Animal Welfare Law (TierSchG). At the GMC, mice were maintained in individually ventilated cages with water and standard mouse chow according to the GMC housing conditions; all tests performed were approved by the responsible authority of the district government of Upper Bavaria, Germany. Mouse experiments at Philipps-University Marburg (Marburg, Germany), were approved by the Regierungspräsidium Giessen, Germany.

Cell culture, plasmids, and viruses

HCT116, H1299, and Saos-2 cell lines were obtained directly from the ATCC (LGC Standards), authenticated in the experiments by p53 genotyping and tested negative monthly for *Mycoplasma* as described previously (32). Primary mouse embryonic fibroblasts (MEF), thymocytes, and splenocytes were isolated and maintained as described previously (16). Transfections and viral infections were performed as described previously (15). For recombinant protein expression in *E. coli*, thermostable p53 (p53TS) constructs (amino acid 41–356; M133L/V203A/N239Y/N268D; refs. 33, 34) were cloned into a pET-15b expression vector with an N-terminal His_{10}-tag followed by a TEV protease cleavage site. Lentiviruses were produced as described previously (16). p53 phospho-variants were generated in pENTR/D-TOPO vector (Invitrogen) with human p53 cDNA using QuickChange Multi Site-Directed Mutagenesis Kit (Agilent) and mutagenesis oligonucleotides listed in Supplementary Table S1. p53 variants were shuttled into pInducer20 and pAdEasy-CMV-Flag (Agilent) vectors using the Gateway System (Invitrogen). pAd–Cas9–Eml4–Alk (24) and pAd–Cas9—Cre–Eml4–Alk (derived from pAd–Cas9–Eml4–Alk by insertion of a Cre-T2A fragment upstream of the FLAG-Cas9 sequence) constructs were used for generation of adenovirus in Ad293 cells (Agilent) as described previously (13).

Thermal shift assay

Thermal shift assay (TSA) was performed to record melting curves with an iCycler iQ PCR Thermal Cycler (Bio-Rad). Proteins were diluted with SEC buffer (25 mM HEPES pH7.5, 150 mM NaCl, 0.5 mM TCEP) to a concentration of 35 μmol/L. A total of 36 μL diluted protein solution was mixed with 4 μL SYPRO Orange dye (Thermo Fisher Scientific) diluted 1:200 in SEC buffer. Samples were transferred into MicroAmp Optical 96-well plates (Thermo Fisher Scientific) and measured every 0.2°C from 22°C to 90°C with an increase of 1°C/minute. The first deviation of the fluorescence signal was normalized and plotted to extract the melting point.

Surface plasmon resonance

DNA binding was measured with the Biacore X-100 system (GE Healthcare) as previously described for the p63 DBD (35). All assays were performed at 20°C and in a modified HBS-P buffer (25 mmol/L HEPES pH7.5, 200 mmol/L NaCl, 0.5 mmol/L TCEP, 0.005% Surfactant P-20). Biotin-labeled 20 bp double-stranded DNA oligonucleotides (Supplementary Table S1) were prepared by annealing the biotinylated forward strand including a T11 tether in a 1:4 ratio with its respective reverse strand. DNA was captured on the streptavidin-coated sensor chip (GE Healthcare) in the respective flow cells until reaching approximately 100 response units. Measurements were performed with a flow rate of 10 μL/minute and included three start-up injections followed by up to 14 injections of p53 with increasing concentrations. Each injection lasted 3 minutes followed by a 3-minute dissociation phase and two injections of regeneration buffer. Data were evaluated using the BIAevaluation software (GE Healthcare) and Prism 8 (GraphPad).

Electrophoretic mobility shift assay and luciferase reporter assays

For electrophoretic mobility shift assay (EMSA), [γ-$_{32}$P]-labeled DNA oligonucleotide (Supplementary Table S1), 5 μL of *in vitro* translated protein, 100 ng α-p53 antibody (Pab421), and 10 pmol unlabeled scrambled oligo were incubated in a total volume of 20 μL of EMSA buffer (20 mmol/L HEPES pH 7.8, 0.5 mmol/L EDTA, 6 mmol/L $MgCl_2$, 60 mmol/L KCl, 0.008% Nonidet P-40, 1 mmol/L DTT, 5% glycerol) supplemented with 120 ng salmon sperm DNA as described previously (13). For luciferase assay, H1299 cells were cotransfected with 200 ng pGL3 reporter plasmid containing a p53 RE, 50 ng phRL-TK plasmid encoding *Renilla* luciferase for

normalization and 100–150 ng p53 expression plasmids (pInducer20); the total amount of DNA per transfection was equalized to 500 ng by addition of pUC19 plasmid. Expression of p53 was induced upon addition of 0.001–0.01 μg/mL doxycycline 6 hours after transfection. Twenty-four hours after transfection, luciferase activities were measured with D-luciferin or coelenterazine using Orion II Microplate Luminometer (Titertek).

CRISPR/Cas9 gene editing

HCT116 *TP53*$^{+/-}$ cells were cotransfected with pX330 (Addgene plasmid, catalog no. 42230) encoding *TP53*-intron5–specific single-guided RNA and a custom-synthesized (Thermo Fischer Scientific) donor DNA for homology-directed repair containing 1,600 bp *TP53* gene sequence (GRCh38/hg38 chr17:7.676.100–7.674.500) with the mutations S183A;S185A (chr.17:7.675.063–7.675.065; chr.17:7.675.057–7.675.059). Transfected cells were expanded as single-cell clones and analyzed by PCR and Sanger sequencing for correct recombination.

Flow cytometry

Bone marrow samples for flow cytometry were collected as described previously (36) and 1 million cells were resuspended in 100 μL MACS buffer (0.5% BSA, 2 mM EDTA in PBS pH7.2) for staining with: biotin-AB Lin cocktail and streptavidin APC-Cy7 (Miltenyi Biotech), FITC CD117 (c-Kit; Biolegend, catalog no. 105805), PE-Cy5 Sca1 (Ly-6A/E; Biolegend, catalog no. 108109), BV 421 CD135 (Flk2; BLD-135313), PE/Dazzle 594 CD34 (BLD-128615). Staining was done as described previously (16) and analyzed using LSRII (BD) cytometer and FlowJo (BD) software. Apoptosis, cell viability, and cell-cycle profile were analyzed as described previously (16).

IHC, immunofluorescence, and Western blot analysis

Sample preparation, immunoblotting, immunofluorescence, and IHC were performed as described previously (15) using: mouse p53 (NCL-p53–505, Leica Microsystems, 1:2,000), human p53 (DO-1, Santa Cruz Biotechnology, 1:2,000], p53 phospho-Ser15 (Cell Signaling Technology, catalog no. 9284, 1:100), cleaved caspase-3 (Cell Signaling Technology, catalog no. 9661, 1:500), cleaved PARP (Cell Signaling Technology, catalog no. 9541, 1:500), p21 (WB: F-5, Santa Cruz Biotechnology, catalog no. sc-6246, 1:200; IHC: #ab188224, Abcam, 1:1,000), BrdU [BU1/75(ICR1), #OBT0030G, 1:100], pErk (E-4, Santa Cruz Biotechnology, 1:100), anti-Ki-67 (TEC-3, DAKO, 1:100), β-actin (AC-15, Abcam, catalog no. ab6276, 1:10,000), Dead-End TM colorimetric TUNEL System (Promega).

ChIP-seq and RNA-seq

Chromatin immunoprecipitation (ChIP) from primary MEFs treated for 16 hours with 0.1% DMSO (control) or 10 μmol/L Nutlin-3a (Nutlin) was done as described previously (16) using anti-p53 antibody (FL393, Santa Cruz Biotechnology) and normal rabbit IgG (Santa Cruz Biotechnology) as the control. ChIP-seq libraries were prepared with the Microplex Library Preparation Kit (Diagenode) according to the manufacturer's instructions. For RNA sequencing (RNA-seq), RNA quality was assessed using the Experion RNA StdSens Analysis Kit (Bio-Rad), libraries were prepared using the TruSeq Stranded mRNA LT Kit (Illumina) according to the manufacturer's instructions, sequenced on the HiSeq 1500 platform (Illumina) in Rapid-Run mode with 50 base single reads and archived at EBI ArrayExpress (E-MTAB-6774, E-MTAB-6793, E-MTAB-9170, E-MTAB-9171).

For ChIP-seq analysis, samples were mapped to the Ensembl Mus musculus reference genome (release 79, GRCm38, mm10) using Bowtie2 (v.2.0.0), aligned reads were deduplicated and subjected to peak calling using MACS (v.1.4) with the sample input as reference. To reduce the number of false-positive ChIP-seq peaks, reported peaks were filtered to retain regions with >3-fold enrichment of read counts compared with input, >50 reads in the sample lane and <50 reads in the input. Blacklisted hyper-ChIPable regions were excluded. Read counts per million were calculated and averaged over all binding sites.

For RNA-seq analysis, reads were mapped as described above and differential expression was assessed using DEseq2 (v.1.14.1). Transcripts per kilobase millions (TPM) were calculated and z-transformed values were depicted as heatmaps. Gene set enrichment analysis (GSEA) was performed using the GSEA software (v.2.1.0) and MSigDB database (v.5.0) using genotype permutation (1,000 permutations) and the signal-to-noise ratio based on TPMs.

Statistical analysis

For statistical analysis, we used GraphPad Prism 8 software. If not stated otherwise, data that were generated by the GMC was analyzed using R (Version 3.2.3). Graphs show mean values obtained with n technical or biological replicates, and error bars in all figures represent SD, unless indicated otherwise. Tests for genotype effects were made by using t tests, Mann–Whitney tests, χ^2 tests or linear models depending on the assumed distribution of the parameter and the questions addressed to the data. Multiple t testing was performed in combination with the FDR approach (two-stage linear step-up procedure of Benjamini and colleagues). P- or FDR q-values <0.05 were used as level of significance.

Results

Phosphomimic mutations of Ser^{183} and Ser^{185} reduce DNA binding and transcriptional activity

Cancer-associated mutations in *TP53* most frequently affect codons that are highly conserved in evolution. Notably, mammalian *TP53* encodes conserved serines next to the H1 helix salt-bridge residues E180 and R181 (**Fig. 1A**). While S185 is missing in rodents, S183 is present in almost all mammals. Nevertheless, cancer-associated mutations that affect codons S183 and S185 of human *TP53* are remarkably rare (**Fig. 1B**). Although there are 35 cases of S183/S185 nonsense or frameshift mutations, there is not a single S183/S185 missense mutation among the 47,005 tumor samples in a curated set of nonredundant The Cancer Genome Atlas (TCGA) studies (37), suggesting no tumor-promoting activity of missense mutations at these codons. This is supported also by the UMD and IARC *TP53* mutation databases: whereas 72.8% of all *TP53* mutations are missense mutations, S183 mutations are nonsense or frameshift mutations in 86.2% (UMD) and 81.1% (IARC). In detail, the UMD database comprises 58,517 *TP53* missense mutations but lists only 18 S183 and 25 S185 missense mutations, yielding a residue-specific mutation frequency of 0.031% and 0.043%, respectively. Likewise, the IARC *TP53* Database for 21,781 cases of somatic *TP53* missense mutations contains records on 9 missense mutations affecting codon S183 (0.041%) and 22 mutations at codon S185 (0.087%). These mutation frequencies are approximately 100-fold lower than codon 175 missense mutations (UMD: 6.3%; IARC: 6.1%) and almost 3- to 8-fold lower than expected by chance (0.25%). The striking underrepresentation of missense mutations at S183/S185, despite evolutionary conservation of these codons, suggested that loss of these serine residues does not promote transformation and is possibly even detrimental for tumorigenesis.

Published OnlineFirst September 1, 2020; DOI: 10.1158/0008-5472.CAN-20-2002

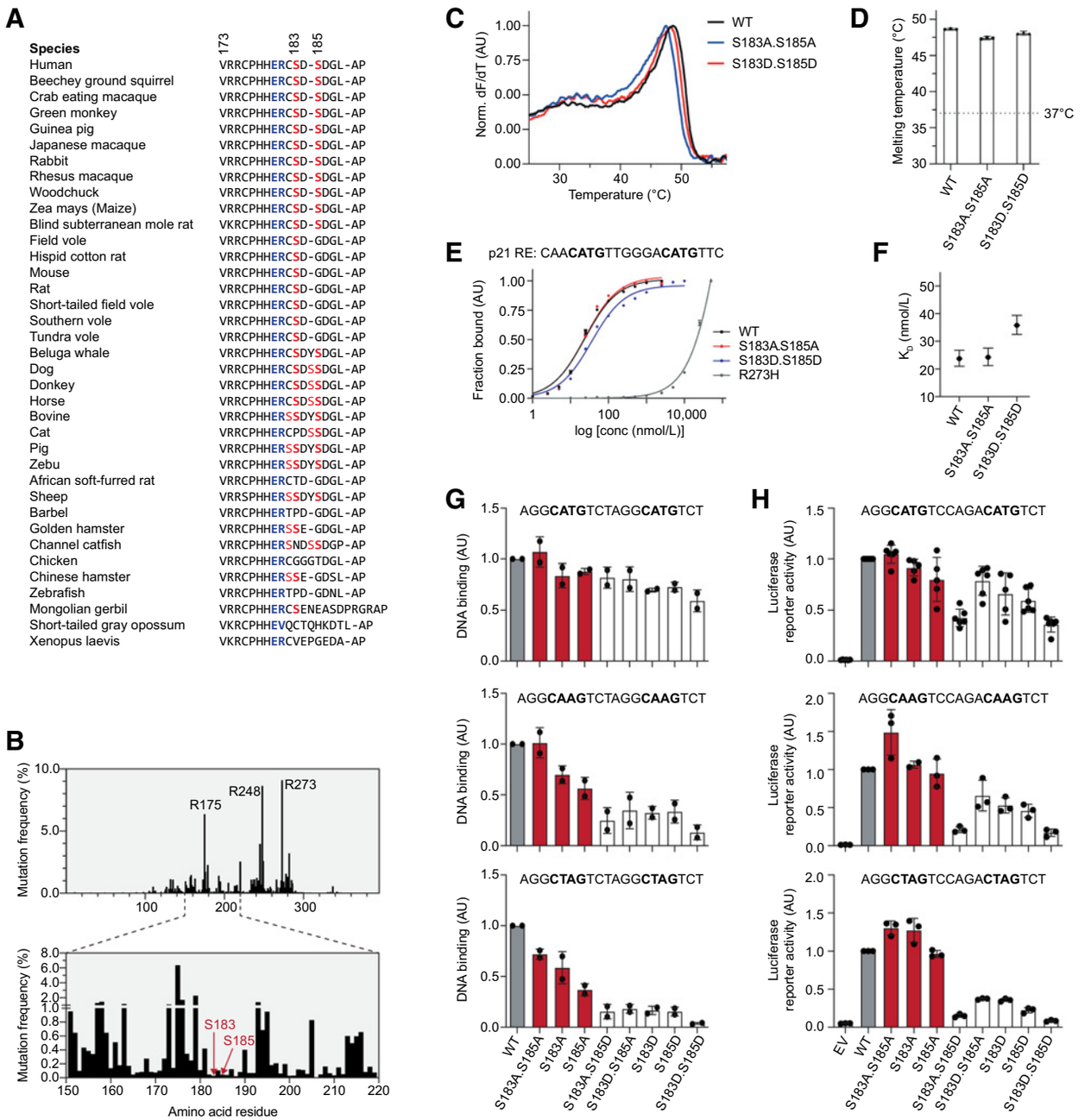

Figure 1.

S183/S185 variants are underrepresented in cancer and affect DNA binding and transcriptional activity. **A,** Evolutionary conservation of serine residues in proximity to helix H1 (aa 176–181). **B,** Spectrum of *TP53* mutations in patients with cancer (UMD database). **C** and **D,** TSA of purified, thermostable p53^{TS}(41–356) variants. **C,** Representative melting curves. Normalized first deviation of the fluorescence intensity is plotted against the temperature. Peak maxima reflect the apparent melting temperature of the protein. **D,** Melting temperatures extracted from melting curves recorded in triplicates. Shown are single data points and mean ± SD. **E** and **F,** SPR affinity curves of p53^{TS}(41–356) variants binding to the p21 RE. The 20 bp core sequence of the p21 RE was immobilized onto a streptavidin-coated chip and a random DNA sequence was used for the reference cell to subtract unspecific DNA binding. Data points were extracted by equilibrium analysis of sensograms and normalized. Plotted triplicates were globally fitted with a nonlinear, least squares regression using a single-exponential one-site binding model. p53 monomer concentration is shown as $\log_{10}$ to resolve all binding curves. **F,** Affinities of p53^{TS}(41–356) variants to the p21 RE. Shown are mean K_D and 95% confidence interval. The K_D of p53 R273H could not be determined as saturation was not reached. **G,** EMSA of *in vitro*–translated full-length p53 proteins and oligonucleotides containing denoted p53 REs. Shown is the intensity of p53 variant DNA complexes normalized to WT p53 as single data points and mean ± SD ($n = 2$). **F,** Luciferase reporter assays. H1299 cells were cotransfected with the indicated p53 variants and luciferase reporter vectors containing different p53 REs. EV, empty vector. Results were normalized to WT and are shown as single data points and mean ± SD ($n = 3$).

Because serine phosphorylation sets a negative charge and has been shown to weaken nearby salt bridges in other proteins (38), we reasoned that it could affect the critical electrostatic interactions between H1 helices and thereby reduce DNA-binding cooperativity. We expressed and purified thermostable p53 (amino acid 41–356) with phosphomimic (S>D) or phospho-deficient (S>A) mutations and the R273H mutant as a negative control (Supplementary Fig. S1A). The melting temperature of the purified proteins was only marginally changed (**Fig. 1C** and **D**), suggesting that S183/S185 phospho-mutations do not change protein folding like many classical tumorigenic mutations that strongly destabilize the structure of the DBD. Measurement of the binding affinity of purified proteins to a p53 RE in the *CDKN1A*/p21 promoter by surface plasmon resonance (SPR) detected a slightly, but significantly reduced affinity for the phosphomimic S183D/S185D (DD) variant, whereas the phospho-deficient S183A/S185A (AA) variant showed a K_D similar to WT p53 (**Fig. 1E** and **F**; Supplementary Fig. S1B).

Next, full-length p53 cDNA constructs with various single and double phosphomimic (S>D or S>E) or phospho-deficient (S>A) codon 183 and 185 point mutations were used for electrophoretic mobility shift assays with oligonucleotides containing high and low affinity p53 REs (**Fig. 1G**; Supplementary Fig. S1C). The binding of phospho-deficient variants were similar to the WT p53 protein. Contrarily, phosphomimic mutations only slightly affected binding to REs with a CATG half site, but strongly reduced binding to CAAG and CTAG half sites, which are bound by WT p53 with high cooperativity (11). The same was previously observed when studying cooperativity mutations affecting residues E180 and R181 (13, 39), supporting the idea that phosphorylation of S183 and S185 reduces DNA binding cooperativity similar to salt bridge mutations.

To analyze how S183/S185 phosphorylation affects transcriptional activity, we examined different phospho-variants in a luciferase reporter assay (**Fig. 1H**; Supplementary Fig. S1D). Consistent with *in vitro* DNA-binding assays, the DD variant displayed the lowest transcriptional activity for all tested REs, whereas the AA variant was transcriptionally at least as efficient as the WT protein (**Fig. 1H**). Importantly, the difference between DD and AA variants was the greatest for reporter constructs containing low affinity REs of proapoptotic targets *TP53AIP1* and *BAX* that are bound by WT p53 with high cooperativity (**Fig. 1H**; Supplementary Fig. S1D). Taken together, our data demonstrate for S183/S185 phosphomimic variants a phenotype remarkably similar to E180/R181 cooperativity mutants, suggesting that phosphorylation of serines adjacent to the H1 helix salt bridge reduces DNA-binding cooperativity, resulting in decreased DNA binding and transcriptional activity.

Phospho-deficient S180A variant displays increased transcriptional activity

S183 from human p53 is conserved in the mouse and corresponds to S180 (**Fig. 1A**). To examine whether constitutive removal of this phosphorylation would affect p53 activity *in vivo*, we generated a phospho-deficient *Trp53*^{S180A} (S180A, SA) knock-in mouse (Supplementary Fig. S2). Homozygous knock-in embryos developed normally. p53 chromatin immunoprecipitation coupled with next-generation sequencing (ChIP-seq) in DMSO- or Nutlin-treated p53$^{+/+}$ and homozygous S180A MEFs revealed a significant enrichment of the canonical p53-binding motif in both genotypes, but the strength of binding was markedly increased in phosphorylation-deficient cells—especially at sites that were only weakly bound by WT p53 (**Fig. 2A–C**). When comparing the sequences of peaks strongly bound by p53 in both WT and knock-in cells to the peaks showing the strongest binding difference between both genotypes, the latter were significantly enriched in sequences that deviate from the canonical p53-binding site and were previously shown to require cooperativity for efficient binding (**Fig. 2D**; refs. 11, 13, 14, 39). In parallel, we analyzed the p53-dependent transcriptome using RNA-seq. In line with the ChIP-seq data, GSEA did not only reveal robust activation of p53 target gene sets in both WT and knock-in cells, but also a small but significant increase in the expression of various curated sets of p53 target genes in S180A as compared with WT cells (**Fig. 2E** and **F**). Furthermore, when Nutlin-activated genes with a binding site in the ChIP-seq dataset were divided into two equal-sized groups with strong (top 50%) versus weak (bottom 50%) binding of p53 (**Fig. 2G**), the average expression in the top was significantly higher than in the bottom for both genotypes, confirming that transactivation correlates with binding intensity (**Fig. 2H**). Of note, expression was significantly higher in S180A than WT MEFs for genes with both strong and weak ChIP-seq signals (**Fig. 2H**), highlighting that the S180A mutation is globally increasing target gene expression.

S180A MEFs have reduced proliferative potential and are senescence prone

We next explored the impact of the S180A variant at the cellular level. Upon γ-irradiation (IR), MEFs of both genotypes showed a similar and transient p53 stabilization (**Fig. 3A**). Induction of target genes was indistinguishable at earlier time points and only slightly increased in some S180A MEFs at 48 hours (**Fig. 3B**), suggesting a minor role of S180 phosphorylation in this setting. Likewise, thymocytes or splenocytes of both genotypes showed similar dynamics of cell death when irradiated *ex vivo* (**Fig. 3C** and **D**).

However, we noted that proliferation of primary S180A embryonic fibroblasts was already exhausted after the second passage, whereas WT cells continued to divide at least 2–3 passages longer (**Fig. 3E**). In line with p53-dependent senescence triggered by unphysiologically high ambient oxygen levels (40), proliferation of WT MEFs was completely rescued at physiologic levels of 3% oxygen (**Fig. 3E**). In contrast, the proliferative potential of S180A cells was extended but eventually still exhausted, suggesting an increased sensitivity to persistent low-level oxidative stress in cell culture. Consistently, also treatment with low doses of doxorubicin, which activates p53 in a reactive oxygen species (ROS)-dependent manner (41, 42), induced a significantly higher number of senescent S180A fibroblasts (**Fig. 3F** and **G**), confirming that S180 phosphorylation deficiency renders MEFs more prone to senescence.

Increased acute stress response in the bone marrow of S180A mice

To explore the *in vivo* response of S180A knock-in mice to acute DNA damage, we subjected mice to whole-body IR. As expected, p53 protein was undetectable under normal conditions (**Fig. 4A**; Supplementary Figs. S3–S5). In irradiated radiosensitive tissues (bone marrow, thymus, spleen, intestine), p53 became quickly stabilized, activated its target Cdkn1a/p21 and rapidly triggered cell death irrespective of genotype (**Fig. 4A–C**; Supplementary Fig. S3A–S3D; Supplementary Fig. S4A and S4B). Of note, the radioresistant organs lung, liver, and kidney remained apoptosis-free also in S180A mice (Supplementary Fig. S5).

Radiation-induced cell-cycle arrest was observed in mice with both genotypes (**Fig. 4D**; Supplementary Figs. S3E and S4C). In the intestine, proliferation resumed after 48 hours with similar kinetics in both genotypes (Supplementary Fig. S4C). In contrast, at this time point, BrdU-positive cells were absent in the thymus and spleen of

Published OnlineFirst September 1, 2020; DOI: 10.1158/0008-5472.CAN-20-2002

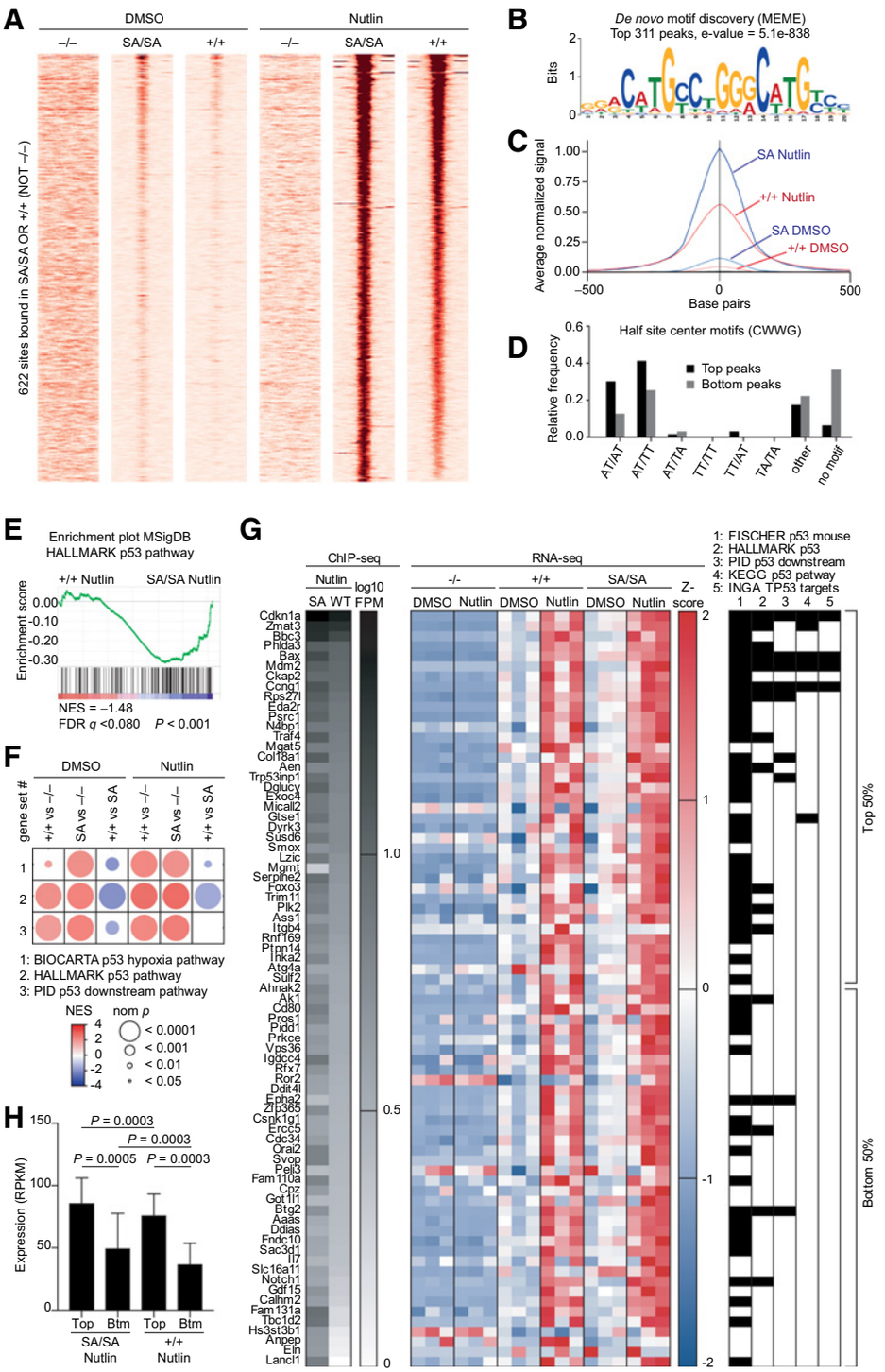

Figure 2.

S180A mutation increases DNA binding and transcriptional activity. **A–D,** p53 ChIP-seq analysis of MEFs ±10 μmol/L Nutlin-3a for 16 hours. **A,** All p53-binding peaks called in Nutlin-treated WT and $p53^{S180A}$ MEFs were merged. Hyper-ChIPable regions also called in $p53^{-/-}$ MEFs were removed, yielding a total of 622 p53-binding peaks, which were sorted from top to bottom by the normalized ChIP-seq signal in Nutlin-treated p53 WT cells. Shown are normalized signal intensities for 2 kb regions surrounding the peak summit. **B,** Motif logo for the best motif discovered with MEME-ChIP in the top 50% of p53-binding sites shown in **A**. **C,** Average signal intensity plots (averaged read count over all genomic regions normalized to the maximum signal) of all binding peaks centered on the peak summit. **D,** Cooccurrence of different dinucleotides at the center of the two p53 RE half sites, that is, the WW positions 5, 6 and 15,16 in the p53RE consensus motif RRRCWWGYYY.RRRCWWGYYY). AA and TT were considered equivalent. Shown are base frequencies at the indicated positions for the top and bottom 10% of p53-binding sites shown in **A**. **E–H,** RNA-seq analysis of untreated and Nutlin-3a–treated low-passage MEFs ($n = 3$ independent MEF preparations per genotype). **E** and **F,** GSEA. **E**, GSEA plot for the MSigDB HALLMARK p53 pathway gene set. **F,** Summary of GSEA results for different p53-related gene sets. NES, normalized enrichment score; nom *P*, nominal *P* value. **G,** Heatmap of p53-activated target genes, that is, all expressed protein-coding genes, which have a p53 ChIP-seq peak and are activated by Nutlin-3a (FC≥1.5) in WT or S180A cells. Shown are z-transformed RNA expression values. Target genes were sorted from top to bottom by the intensity (log_{10} FPM, fragments per million) of the p53 WT ChIP-seq peak (left). Genes included in p53-related gene sets are labeled in black (right). **H,** Expression of the $n = 37$ top and 38 bottom p53-activated target genes from **G** in Nutlin-3a–treated WT or S180A MEFs. Shown is the mean ± SEM (two-tailed Mann–Whitney test); RPKM, reads per kilobase of exon per million reads mapped.

S180A mice, while first proliferating cells were clearly detectable in WT animals (Supplementary Fig. S3E). Likewise, we observed significantly lower numbers of BrdU-positive cells in S180A versus WT bone marrow samples 72 hours after IR, despite similar induction of apoptosis (**Fig. 4D** and **E**). Together, these differences indicated a higher sensitivity of hematopoietic S180A cells and suggested defects in restoration of hematopoiesis after DNA damage.

We therefore analyzed the hematopoietic compartment in more detail. In the absence of exogenous genotoxic stress, S180A mice showed a pronounced reduction in total bone marrow cellularity, which was accompanied by a somewhat increased, but not reduced number of $Lin^{-/low}$, $Sca1^{+}$, c-Kit^{+} (LSK) hematopoietic stem cells (HSC) and LSK, $CD34^{-}$, $Flk2^{-}$ long-term (LT) HSCs (**Fig. 4F**; Supplementary Fig. S6A). Together with a slightly

Published OnlineFirst September 1, 2020; DOI: 10.1158/0008-5472.CAN-20-2002

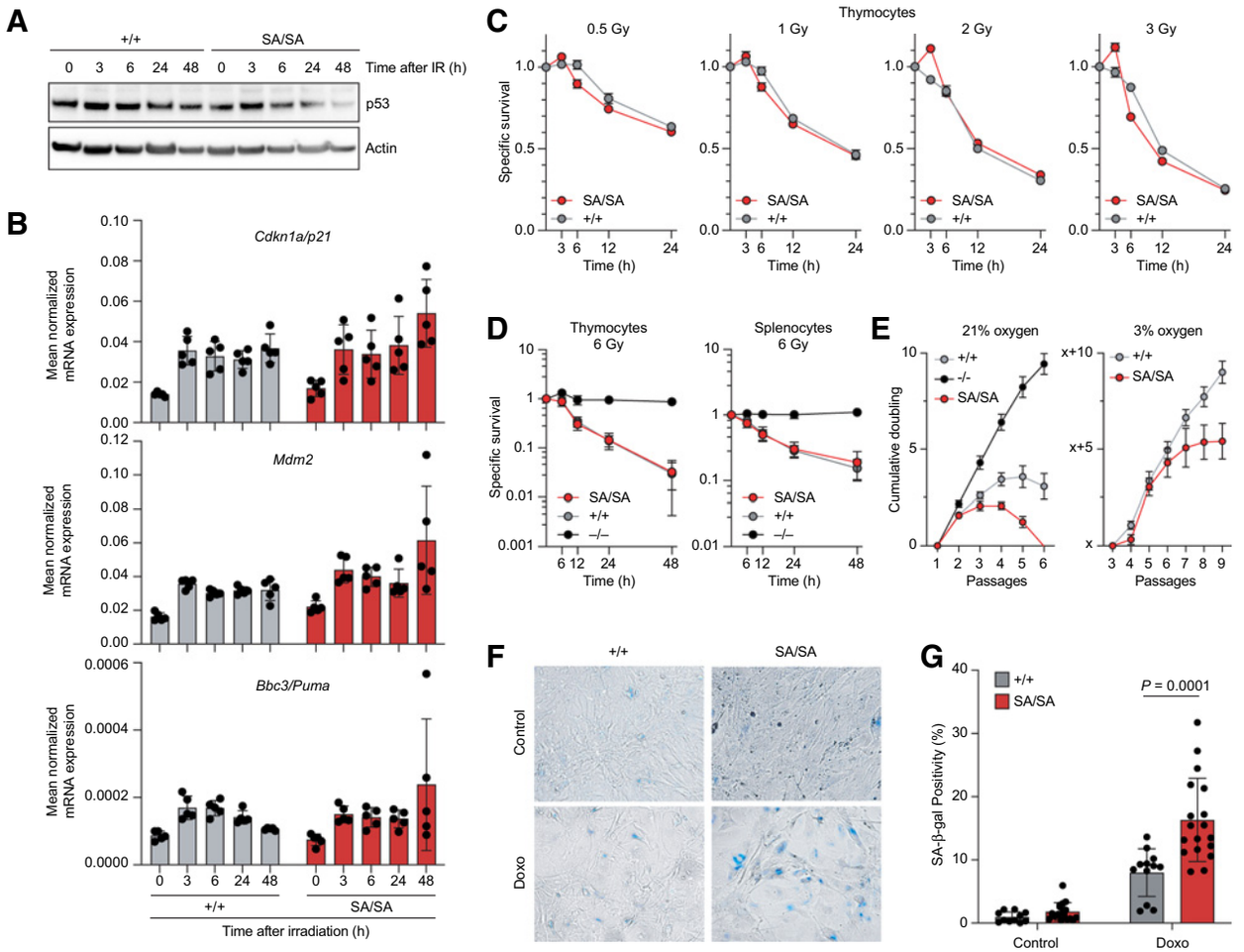

Figure 3.

S180A reduces proliferative potential and enhances senescence. **A** and **B,** Early passage $p53^{+/+}$ (+/+) and homozygous S180A (SA/SA) MEFs were irradiated with 6 Gy. **A,** Western blot. **B,** Quantitative RT-PCR for indicated p53 target genes. Shown is expression normalized to β-actin as mean ± SD ($n = 5$ batches of MEFs per genotype). **C** and **D,** Primary thymocytes or splenocytes were irradiated *ex vivo*. Shown is specific survival as mean ± SD ($n = 3$ per genotype for each dose and time point). **E,** Proliferative potential of MEFs with indicated genotypes cultured at ambient (21%) or physiologic (3%) oxygen level. Shown are cumulative population doublings. **F** and **G,** Low-passage primary MEFs from littermates ($n = 3$ per genotype; $n = 6$ replicates each) were treated at low passage with low-dose doxorubicin (50 ng/mL) for 48 hours and stained for senescence-associated β-galactosidase (SA-β-gal). **F,** Representative images. **G,** Percentage of SA-β-gal–positive cells. Shown are single data points and mean ± SD (unpaired, two-sided *t* test).

reduced proportion of lymphoid and increased percentage of myeloid cells in the peripheral blood of S180A mice (Supplementary Table S2), these data remind of an "aged hematopoietic phenotype," which is characterized by a reduced functionality of LT stem cells (LT-HSC; ref. 43). To test the regenerative ability of the LT-HSC, we performed myeloablation experiments with 5-fluorouracil (5FU; ref. 44). 5FU eliminates fast proliferating short-term progenitor cells, sparing LT-HSC, which survive and ensure recovery of hematopoiesis by replenishing the progenitor pools. As expected, one week after 5FU injection we detected in both groups a marked drop in the blood leukocyte count (**Fig. 4G**). A total of 12 days after treatment, the number of leukocytes was restored to almost normal in WT mice, whereas leukocyte counts did not recover in S180A animals, pointing to an impaired functionality of HSCs (**Fig. 4G**). In principle, the observed regenerative defect can be explained by a higher sensitivity of S180A stem cells to 5FU, which would lead to a reduction in the LT-HSC pool and failure in reconstitution of the progenitor population after treatment. In support of this hypothesis, 12 days after 5FU injection activation of stem cells led to an increase of the total LSK population in WT animals, but not in S180A mice (**Fig. 4H**). Concomitantly, the number of LT-HSCs was strongly reduced in S180A animals relative to WT (**Fig. 4H**; Supplementary Fig. S6B).

Inspired by the HSC phenotype, we also assessed the regenerative capacity of tissue-specific stem cells in the muscle. By direct intramuscular injection of $BaCl_2$, we induced muscle injury, which was subsequently repaired by activation of satellite stem cells. Tissue samples obtained at different time-points after $BaCl_2$ application showed a substantially larger necrotic area 4 days after injection and a delayed recovery of muscle tissue after 12 days in S180A compared with WT mice (Supplementary Fig. S7).

Published OnlineFirst September 1, 2020; DOI: 10.1158/0008-5472.CAN-20-2002

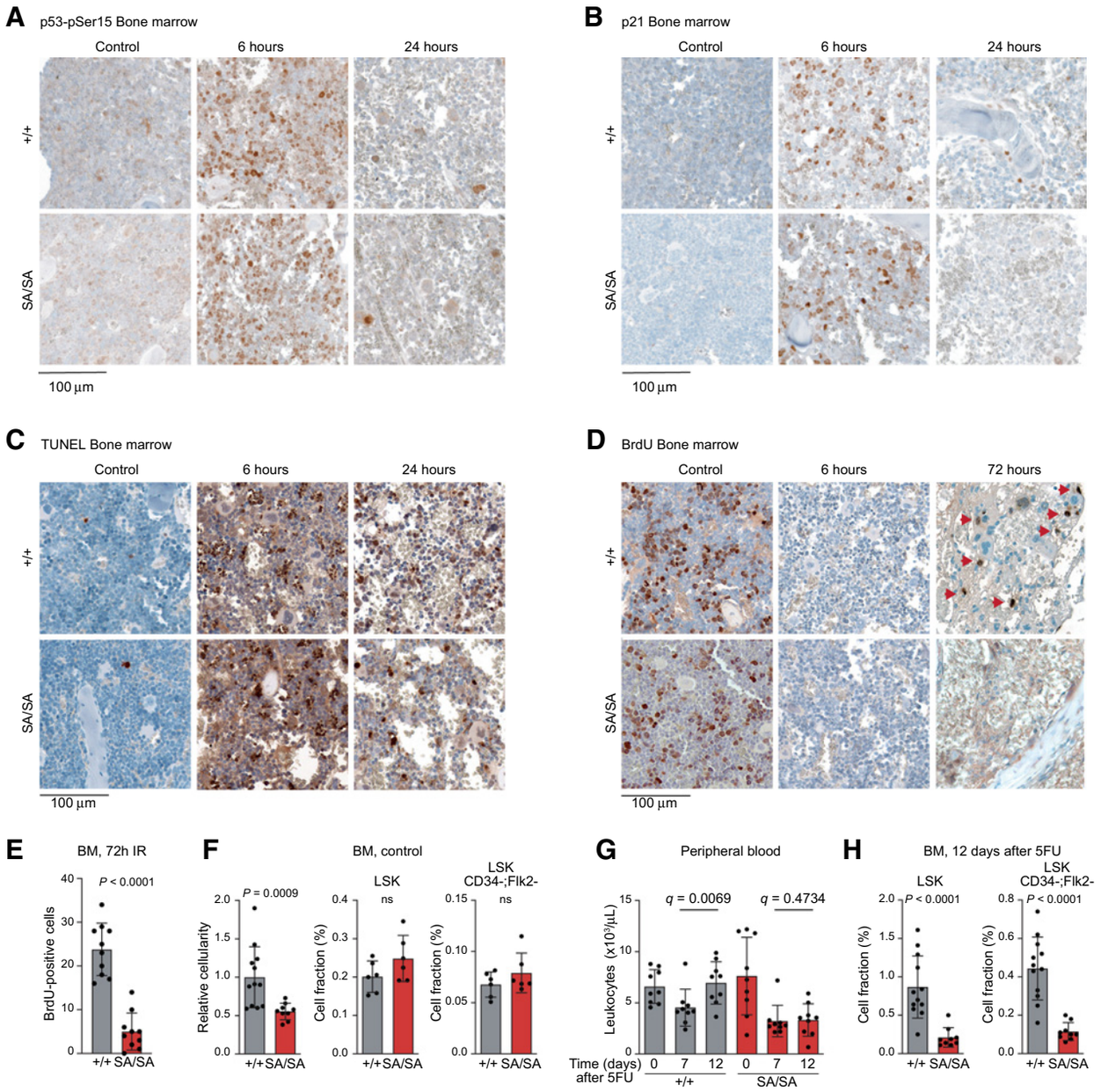

Figure 4.

Delayed recovery of hematopoietic compartment from DNA damage in S180A mice. **A–E,** Whole-body irradiation (6 Gy) of $p53^{+/+}$ (+/+) and homozygous S180A (SA/SA) mice. IHC of bone marrow for p53-pSer15 (**A**), p21/Cdkn1a (**B**), apoptosis/TUNEL (**C**), and proliferation/BrdU (**D**). **E,** Shown is the number of BrdU-positive cells 72 hours after IR in 500 × 500 μm^2 fields of view. Two-sided Mann–Whitney test ($n = 3$ mice per genotype with 2–4 samples per mouse). **F,** Flow cytometry analysis of bone marrow from femurs of untreated mice after removal of erythrocytes. Left, total cellularity of SA/SA samples ($n = 10$) normalized to the mean of +/+ samples ($n = 12$). Middle and right, fraction of $Lin^{-/low}$, $Sca1^{+}$, c-kit^{+} (LSK) and LSK, $CD34^{-}$, $Flk2^{-}$ cells ($n = 6$ per genotype). Two-sided Mann–Whitney test. The gating strategy is shown in Supplementary Fig. S5. **G,** Total leukocyte concentration of peripheral blood collected at indicated time points before and after 5FU treatment of mice. Multiple two-sided *t* tests in combination with the FDR approach. Reported are FDR *q*-values ($n = 9$ per time point and genotype). **H**, Flow cytometry analysis of bone marrow samples 12 days after 5FU treatment as described in **F**. Two-sided Mann–Whitney test ($n = 12$ for +/+, $n = 10$ for SA/SA). All graphs show individual data points and mean ± SD.

These experimental data indicate that loss of p53 S180 phosphorylation causes an impairment in tissue regeneration. This phenotype is particularly prominent in the bone marrow, which highlights the importance of phosphorylation-mediated inhibition of p53 activity for preservation of HSC function.

S180A mice show reduced longevity

To better understand the impact of the S180A mutation in the context of the complete organism, we performed deep phenotype analysis on large cohorts of homozygous S180A knock-in and WT littermates (Supplementary Table S3). Prenatal and postnatal

Published OnlineFirst September 1, 2020; DOI: 10.1158/0008-5472.CAN-20-2002

Table 1. Necropsy results.

Major pathology	+/+		SA/SA	
Neoplasm	10	32.3%	8	18.6%
Nonspecific systemic disease[a]	15	48.4%	26	60.5%
Ocular lesion[b]	3	9.7%	3	7.0%
Other[c]	1	3.2%	4	9.3%
Unknown	2	6.5%	2	4.7%
Total number of examined animals	31	100%	43	100%

[a]Nonspecific systemic disease: age-related or -induced lesions including cardiac and respiratory failure, sepsis and DIC, female reproductive diseases or male urogenital diseases, etc.
[b]Ocular lesion: includes corneal ulceration and chronic keratitis.
[c]Other: includes rectal prolapse, gastrointestinal bleedings, megaesophagus, nephropathy.

development of homozygous animals did not differ from WT littermates, and by the age of 7–20 weeks they had similar bodyweight, no dysmorphology and no significant alterations in the structure of inner organs (Supplementary Tables S3 and S4). Also, physiologic parameters such as cardiovascular and muscle function, energy metabolism, body temperature, behavior, and perception were unaffected in homozygous S180A mice (Supplementary Table S4). Clinical chemistry analysis of blood did not show substantial differences between young adult S180A and WT animals (Supplementary Table S2). Detailed hematologic and immunologic examinations revealed a slight decrease in lymphocytes and increase in granulocyte populations in knock-in females, whereas in males this tendency did not reach statistical significance (Supplementary Table S2). Thus, we did not detect any major structural or physiologic differences in S180A mice, indicating that in normal conditions S180 phosphorylation has only minute effects at most on p53′s functions *in vivo*.

However, it is well established that maintenance of different stem cell compartments is critical for longevity and that elevated p53 activity in mice can compromise stem cell function, resulting in aging (44–47). When aging cohorts of mice, we noticed that the median overall survival of homozygous S180A was significantly shorter than that of WT mice—568 versus 709 days, respectively (**Fig. 5A**). Interestingly, several parameters known as markers of aging in mice, such as body

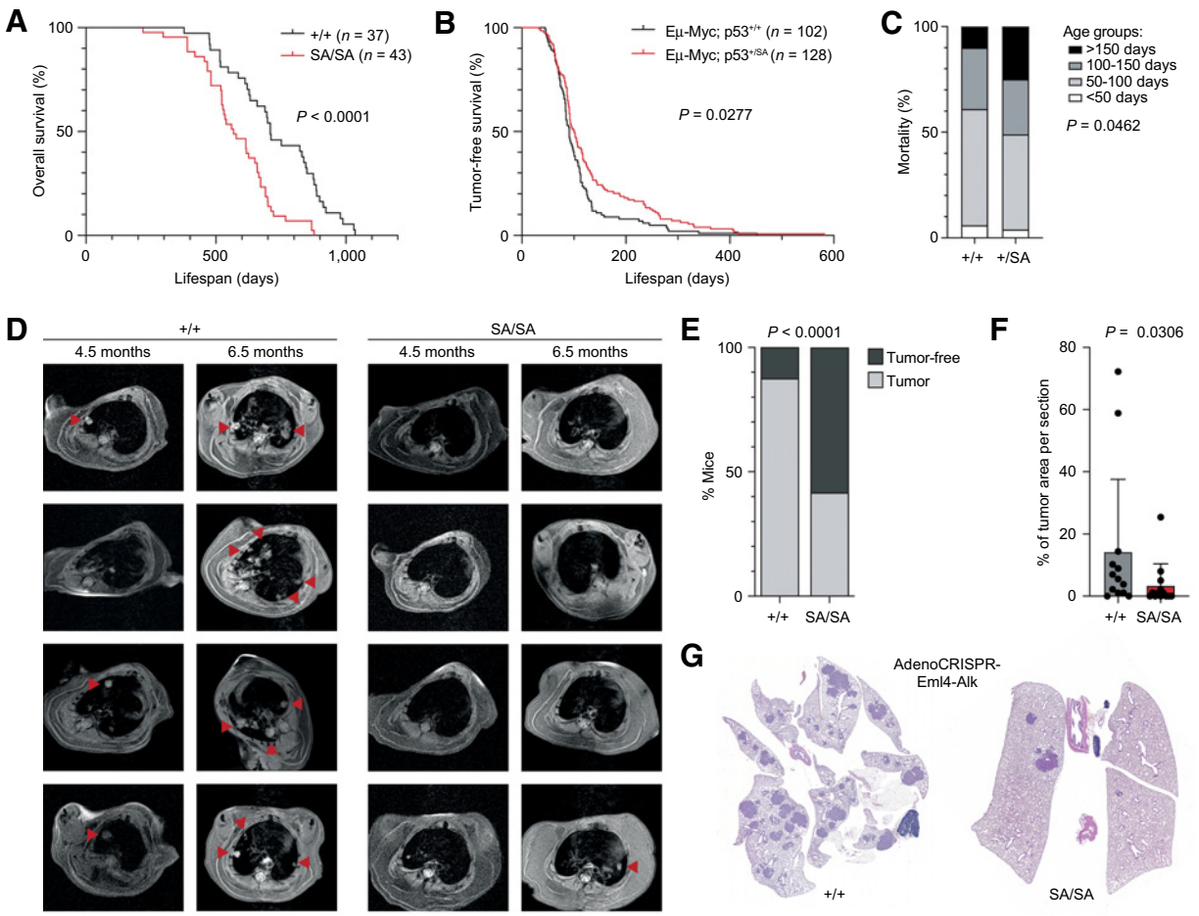

Figure 5.
Reduced lifespan and enhanced tumor suppression in S180A mice. **A,** Kaplan–Meier plots for overall survival (log-rank test). **B–C,** *Myc*-driven B-cell lymphoma in $p53^{+/+}$ and $p53^{S180A}$ mice. **B,** Kaplan–Meier plots for tumor-free survival (log-rank test). **C,** Mortality in different age groups (χ^2 test). **D–G,** *Eml4–Alk*-driven non–small cell lung cancer in $p53^{+/+}$ and $p53^{S180A}$ mice. **D,** Lung MRIs of four representative mice of each group at indicated time points after infection with *Eml4–Alk* CRISPR adenovirus. Arrowheads, tumors. **E,** Percentages of tumor-free animals at last BLI before $p53^{+/+}$ control animals reached the endpoint. **F,** Percentage of tumor area relative to total area per section (Mann–Whitney test, $n = 13$ per genotype). **G,** Representative hematoxylin and eosin–stained lung sections.

Published OnlineFirst September 1, 2020; DOI: 10.1158/0008-5472.CAN-20-2002

weight, lordokyphosis (spinal curvature), and dermal thickness, did not show significant differences (Supplementary Fig. S8). Instead, premature death of S180A mice was accompanied by a general loss of fitness and nonspecific systemic diseases such as age-related cardiac and respiratory failure also seen in older WT animals, but not linked to a particular pathology (**Table 1**). We conclude that in the absence of exogenous genotoxic stress S180A mice have a largely normal phenotype, but show a markedly reduced lifespan resulting from nonspecific, age-related systemic diseases.

Loss of S180 phosphorylation enhances tumor suppression

A reduction in DNA-binding cooperativity compromises p53′s tumor-suppressive function (15, 16), prompting us to hypothesize that the increased cooperativity of S180A potentiates tumor suppression. Indeed, we observed a reduction in neoplastic diseases in aged S180A mice (32.3% in WT vs. 18.6% in S180A mice; **Table 1**). To exclude that the tumor incidence is simply reduced because of the shortened lifespan, we explored resistance to experimentally enforced, oncogene-driven tumorigenesis using genetically-engineered mouse models of malignant lymphoma and lung cancer.

In the Eμ-*Myc* lymphoma model, enforced overexpression of a *Myc* transgene induces B-cell lymphoma with 100% penetrance (23), and the latency of disease is strongly dependent on p53 status (48). Eμ-*Myc* transgenic mice with a single S180A allele demonstrated a superior median lifespan in comparison with $p53^{+/+}$ littermates (103 vs. 91 days, $P < 0.0277$; **Fig. 5B**). The proportion of long-lived mice, who remained tumor-free longer than 150 days, was more than 2.5-fold higher in the S180A cohort than in the WT group (**Fig. 5C**). More than 25% of S180A mice, compared with only 10% of WT animals, remained lymphoma-free at this time point (**Fig. 5C**). Hence, Myc-induced lymphomagenesis was substantially delayed in the absence of S180 phosphorylation.

To assess whether loss of S180 phosphorylation also augments p53-mediated tumor suppression in solid tumors, we used a mouse model for Anaplastic Lymphoma Kinase (*ALK*)-positive non–small cell lung cancer, in which prognosis is strongly affected by p53 status (24, 49, 50). When inducing an *Eml4–Alk* fusion oncogene by intratracheal adenoviral delivery of CRISPR/Cas9 nucleases (24), S180A mice displayed pronounced resistance to *Eml4-Alk*-driven tumorigenesis (**Fig. 5D**). Seven of 12 (58%) S180A mice were still tumor-free, when 14 of 16 (88%) WT mice already presented tumors (**Fig. 5E**). When the animals were analyzed histologically at the experimental endpoint, the overall tumor burden was significantly reduced in S180A mice and 46% of S180A samples were completely tumor-free and displayed only small hyperplastic foci (**Fig. 5F** and **G**). The levels of phospho-ERK as a marker for Eml4–Alk activity and the proliferation marker Ki-67 in tumors from S180A and WT mice were similar (Supplementary Fig. S9), suggesting that loss of S180 phosphorylation potentiated the tumor-suppressive function of p53 at early stages of tumorigenesis, but did not change the tumor phenotype—possibly because p53 functions become blunted in established tumors. In conclusion, two independent mouse models of oncogene-driven hematopoietic and lung cancer indicate that loss of S180 phosphorylation can enhance tumor suppression by p53.

Human S183/S185 phosphorylation deficiency enhances p53-mediated tumor cell apoptosis

To estimate whether phosphorylation-dependent regulation of cooperativity is also relevant for tumor-suppressive p53 functions in human cancer cells, we expressed various phosphomimic and phospho-deficient S183/S185 variants in p53-deficient Saos-2 cells (**Fig. 6A** and **B**). While all variants were mounting a cell-cycle arrest to similar extent as WT, phosphomimic variants were impaired in triggering apoptosis—similar to various low-cooperativity variants with mutations of the H1 helix salt bridge residues E180 and R181 (13, 39).

To analyze apoptotic functions of the phospho-variants in a more physiologic setting, we introduced the phospho-deficient S183A/S185A (AA) and phosphomimic S183D/S185D (DD) point mutations into HCT116 $TP53^{+/-}$ colon cancer cells by CRISPR/Cas9-mediated genome editing. Correct *TP53* gene editing was confirmed by sequencing of exon 5 and full-length p53 cDNA (**Fig. 6C**). Similar to WT, the AA and DD variants displayed normal nuclear localization and stabilization after treatment with the Mdm2 inhibitor Nutlin-3a or upon genotoxic stress (**Fig. 6D** and **E**). Multiple independent clones of HCT116-AA cells showed enhanced DNA damage–induced target gene expression, whereas HCT116-DD clones were transcriptionally compromised compared with $HCT116^{+/-}$. Furthermore, compared with both WT and HCT116-DD cells, HCT116-AA clones demonstrated superior induction of apoptosis in response to doxorubicin (**Fig. 6E** and **F**). Taken together, our results indicate that $p53^{S183/S185}$ phosphorylation limits the tumor-suppressive, proapoptotic p53 activity in human cancer cells, strongly suggesting that targeting this phosphorylation could synergize with p53-activating drugs and improve cancer therapy responses.

Discussion

p53 suppresses tumorigenesis primarily as a transcription factor that binds DNA cooperatively as a tetramer. Cooperative DNA binding is supported not only by the dedicated oligomerization domain but also by interactions mediated by the DNA-binding core domains—in particular, via salt bridges between the H1 helix residues E180 and R181 (17–20). These salt bridges are indispensable for tumor suppression as proven by the increased cancer susceptibility of E180/R181 mutant knock-in mice and an estimated worldwide number of 34,000 patients with cancer per year with salt-bridge mutations (15, 16, 21). Whether and how p53 DNA-binding cooperativity is regulated, however, remained elusive.

Here, we provide evidence that DNA-binding cooperativity is influenced by serine residues (S183 and S185 in human p53 and S180 in mouse p53) in direct proximity to the salt bridge. While PTMs of p53 typically cluster in the intrinsically unstructured N- and C-terminal regions of the protein and are only rarely observed in the DNA-binding core domain, several independent mass spectrometry studies have provided evidence for S183/S185 phosphorylation (5–8). As phosphorylation sets a negative charge, we hypothesize that the altered surface charge distribution pattern affects the core domain interactions that are critical for DNA-binding cooperativity. Supporting this assumption, it has been recently demonstrated for Raf Kinase Inhibitory Protein that phosphoserine in the vicinity of an intermolecular lysine-glutamate salt bridge competes for the lysine, initiating a partial unfolding event that leads to the dissociation of the salt bridge (38). In addition, it is interesting to note that many S183/S185 phosphorylated peptides identified by mass spectrometry are also R181 methylated (7, 8). Given substantial evidence for interdependent posttranslational protein modification by protein arginine methyltransferases and kinases (including Aurora B; refs. 51–53), it is tempting to speculate that sequential or concurrent methylation of R181 reinforces disruption of the E180-R181 salt bridge.

Multiple phosphomimetic (S-to-D or S-to-E) p53 variants showed a marked reduction in DNA binding and transactivation, which was evident most clearly at REs that deviated from the consensus motif

Published OnlineFirst September 1, 2020; DOI: 10.1158/0008-5472.CAN-20-2002

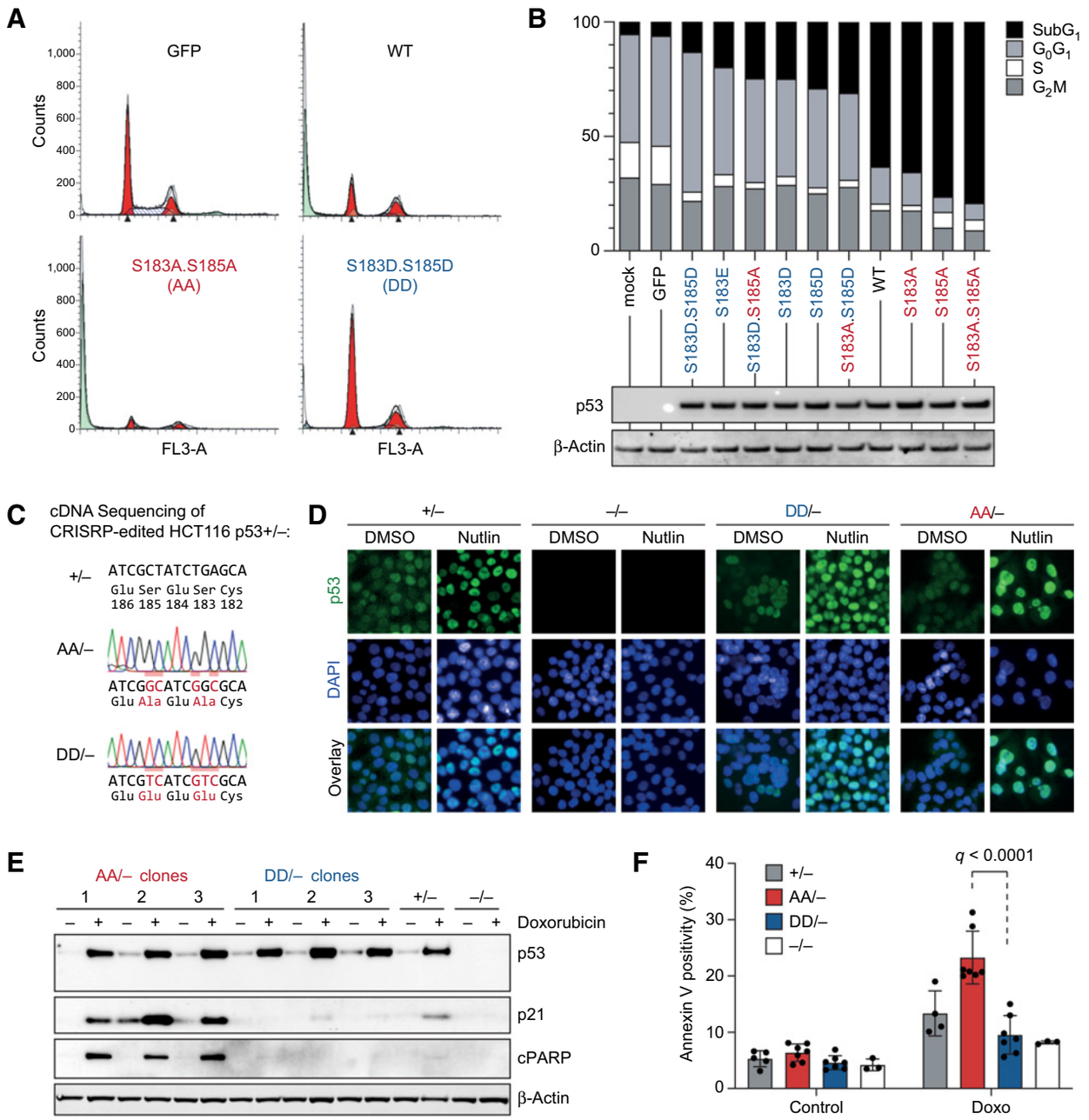

Figure 6.

S183/S185 phosphorylation deficiency sensitizes human cancer cells to p53-mediated apoptosis. **A** and **B,** p53-null Saos-2 osteosarcoma cells were infected with adenovirus expressing different $p53^{S183/S185}$ phospho-variants (red, phospho-deficient; blue, phosphomimic) and WT p53 or GFP as controls. **A,** Representative cell-cycle profiles. **B,** Quantification of cell-cycle phase distribution by ModFit analysis. Bottom, Western blot analysis documenting comparable expression of all p53 variants. **C–E,** HCT116 $p53^{+/-}$ cells were targeted with CRISPR technology to express the S183A.S185A (AA) and S183D.S185D (DD) variants from the endogenous *TP53* gene locus. **C,** cDNA sequencing results (reverse strand) of a representative AA/– and DD/– clone. **D,** Representative p53 immunofluorescence images of indicated cell lines untreated and treated 16 hours with 10 μmol/L Nutlin-3a. **E,** Western blot analysis of different independent cell clones untreated and 24 hours after treatment with 0.25 μg/mL doxorubicin. HCT116 $p53^{+/-}$ and $p53^{-/-}$ cells are shown as controls. **F,** Quantification of apoptosis by Annexin V flow cytometry. Cell clones of indicated p53 genotypes were treated 24 hours with 0.25 μg/mL doxorubicin or left untreated (control). Shown are individual data points and mean ± SD; FDR *q*-values of multiple two-sided *t* tests in combination with the FDR approach.

(**Fig. 1G** and **H**). The resulting restriction of the target gene spectrum to the most consensus-like REs translated into a reduced induction of apoptosis (**Fig. 6**), that is highly characteristic also for cooperativity mutations affecting E180 and R181 (13, 14, 39), further supporting the idea that S183/S185 phosphorylation reduces DNA-binding cooperativity. Of note, while S183 phosphorylation has been linked previously

Published OnlineFirst September 1, 2020; DOI: 10.1158/0008-5472.CAN-20-2002

to accelerated p53 degradation through the polyubiquitination–proteasome pathway (5), we did not observe reduced expression levels for phosphomimic variants despite pronounced changes in p53 activity (**Fig. 6B** and **D**; Supplementary Fig. S1D).

Phosphorylation-deficient S-to-A variants displayed a strongly tissue and context-dependent phenotype. Possibly due to an absence of phosphorylation in recombinant p53, phosphorylation-deficient S-to-A variants did not show increased DNA binding *in vitro* (**Fig. 1**; Supplementary Fig. S1). When expressed from the endogenous *Trp53* gene locus, the mouse S180A variant activated classical p53 target genes in irradiated MEFs (**Fig. 3B**) and induced apoptosis in irradiated lymphocytes similar to WT (**Fig. 3C** and **D**). Moreover, when S180A mice were X-irradiated, the degree and extent of IR-induced apoptosis was not increased (**Fig. 4C**; Supplementary Figs. S3D and S4B) and tissues, in which IR does not induce apoptosis, remained radioresistant (Supplementary Fig. S5). However, pronounced differences were observed in response to chronic stress and with regard to proliferation. The oxidative stress-dependent senescence of primary MEF cultures was accelerated and enhanced in the S180A genotype (**Fig. 3F** and **G**) and proliferation in the thymus, spleen, and bone marrow failed to resume properly after DNA damage (**Fig. 4D**; Supplementary Fig. S3E), resulting in defective recovery from neutropenia (**Fig. 4G** and **H**). Overall, this fairly selective hematopoietic phenotype is likely reflecting the exceptional vulnerability of bone marrow stem cells to elevated p53 activity that is also responsible for the bone marrow toxicity observed in patients treated with Mdm2 inhibitors and in mice with deregulated p53 activity (46, 54–58). Importantly, this phenotype suggests that S180 phosphorylation has a critical role in dampening DNA damage–triggered p53 activity to preserve the HSC compartment.

Although young S180A mice did not display any significant differences to WT animals (Supplementary Tables S2–S4), we observed a marked reduction in lifespan (**Fig. 5A**). This is reminiscent of early aging phenotypes reported for several mouse models with elevated p53 activity (44–47). However, aging is not a default phenotype resulting from elevated organismal p53 activity as demonstrated by multiple mouse models with enhanced p53-mediated tumor suppression in the absence of premature aging (57, 59). Interestingly, $p53^{TSD/-}$ mice with the T21D/S23D mutation, that mimics constitutive phosphorylation of the p53 N-terminus, die by 6 weeks of age exhibiting accelerated aging, which is rescued by deletion of the proapoptotic p53 target gene *Bbc3*/*Puma* (46). In striking contrast to this aging-promoting effect of N-terminal phosphorylation, DBD phosphorylation at S180 counteracts premature aging and therefore represents the first PTM of p53 that increases longevity.

Different from mice with aberrant expression of N-terminally truncated p53 (44), the aging phenotype in S180A mice appeared as a more subtle predisposition to premature death by cardiac or respiratory failure without gross alterations in body weight, dermal thickness, or osteoporosis-associated lordokyphosis (**Table 1**; Supplementary Fig. S8). A possible explanation is the rather selective increase of p53 activity in the hematopoietic compartment of S180A mice (**Fig. 4**). It can be envisioned that the exceptional vulnerability of HSCs to everyday genotoxic insults progressively depletes the HSC pool and, as p53 activity is controlling clonal competition in the bone marrow (60), eventually decreases the clonal complexity in the bone marrow. Of note, the most extreme form of a reduced HSC clonal complexity, clonal hematopoiesis of indeterminate potential (CHIP) in the elderly, results in an increased risk of all-cause and cardiovascular mortality likely via its effects on immune function (61). We therefore speculate that the loss of HSC function indirectly compromises other tissues thereby predisposing to a broad range of age-related disorders that reduce the lifespan.

Similar as in other mouse models with elevated p53 activity (44, 59), we also observed improved resistance to spontaneous (**Table 1**) and oncogene-enforced tumorigenesis (**Fig. 5**). In established tumor cell lines, enforced expression of nonphosphorylatable S183/S185 variants triggered apoptosis more effectively than WT p53 and CRISPR-engineered S183/S185-to-A mutations of the endogenous *TP53* gene locus sensitized to chemotherapy-induced apoptosis (**Fig. 6**). *Vice versa*, phosphomimic S183/185 mutations reduced p53-mediated apoptosis, suggesting that such mutations would be tumorigenic. However, single-nucleotide substitutions cannot change these serine codons (TCA or AGC) to Asp or Glu (GAN), providing an explanation why S183/S185 missense mutations are underrepresented in patients with cancer and phosphomimic mutations at these codons have not been described (**Fig. 1B**). Together these results reinforce the notion that S183/S185 phosphorylation is not only promoting tumorigenesis but also required for tumor maintenance. Importantly, this suggests inhibition of S183/S185 phosphorylation as a new potential treatment strategy to enhance the proapoptotic function of p53 for tumor therapy. Although the role of S183/S185 phosphorylation has not been studied in the context of mutant p53, it is tempting to speculate that targeting this phosphorylation might not only boost WT p53 activity but also rescue some p53 mutants. This might apply in particular to nonhotspot mutants, many of which retain a residual level of DNA binding activity, that might be increased to WT levels through improved cooperativity.

Unfortunately, the S183/S185 kinases remain poorly characterized. S183 (mouse S180) is a predicted consensus site for Aurora kinases. Aurora A is known to reduce p53 activity by phosphorylating multiple sites different from S183/S185 (62–64). Aurora B has also been reported to phosphorylate p53 at several sites, including S183 (5, 6). Moreover, Aurora A and B were both identified as kinases essential for pluripotency in embryonic stem cells (65). Furthermore, analysis of the TCGA PanCancer Atlas reveals a mutual exclusivity of inactivating *AURKB* alterations (deep deletions and missense mutations) with WT p53 status (Supplementary Fig. S10), suggesting that Aurora B might be required for attenuating WT p53 function in tumors. Although mass spectrometry has provided evidence for S185 along with S183 phosphorylation (7, 8), a S185 kinase has not yet been reported. To exploit the therapeutic potential of boosting the apoptotic activity of p53, it will therefore be of utmost importance to systematically identify the kinases responsible for S183/S185 phosphorylation in tumor cells.

In summary, our study provides evidence at the biochemical, cellular, and organismal level that p53 functions in tumorigenesis and aging are balanced at the level of DNA-binding cooperativity by serine phosphorylation.

Disclosure of Potential Conflicts of Interest

V. Dötsch reports grants from DFG during the conduct of the study. Hrabé de Angelis reports grants from Bundesministerium für Bildung und Forschung (Projektbezogene Förderung Nummer 01KX1012) during the conduct of the study. T. Stiewe reports grants from Deutsche Forschungsgemeinschaft, Deutsche Krebshilfe, Deutsche José Carreras Leukämie Stiftung e.V., German Center for Lung Research (DZL), von Behring-Röntgen Stiftung, and Bundesministerium für Bildung und Forschung during the conduct of the study, and grants from Universitätsklinikum Giessen and Marburg outside the submitted work. No potential conflicts of interest were disclosed by the other authors.

Authors Contributions

O. Timofeev: Conceptualization, data curation, formal analysis, supervision, funding acquisition, validation, investigation, visualization, methodology, writing-original draft, project administration. **L. Koch:** Formal analysis, investigation, writing-review and editing. **C. Niederau:** Formal analysis, investigation, writing-

review and editing. **A. Tscherne:** Formal analysis, investigation, writing-review and editing. **J. Schneikert:** Formal analysis, investigation, writing-review and editing. **M. Klimovich:** Formal analysis, investigation, writing-review and editing. **S. Elmshäuser:** Formal analysis, supervision, investigation, project administration, writing-review and editing. **M. Zeitlinger:** Formal analysis, investigation, writing-review and editing. **M. Mernberger:** Data curation, software, formal analysis, writing-review and editing. **A. Nist:** Formal analysis, investigation, writing-review and editing. **C. Osterburg:** Formal analysis, investigation, writing-review and editing. **V. Dötsch:** Formal analysis, supervision, writing-original draft, writing-review and editing. **German Mouse Clinic Consortium:** Formal analysis, investigation, writing-review and editing. **M. Hrabé de Angelis:** Supervision, funding acquisition, writing-original draft, project administration, writing-review and editing. **T. Stiewe:** Conceptualization, supervision, funding acquisition, writing-original draft, project administration, writing-review and editing.

Acknowledgments

Authors thank Sigrid Bischofsberger, Antje Grzeschiczek, Angela Mühling, Björn Geissert, Franziska Wojciech, Saumya Manmadhan and employees of the animal facility of Marburg University for technical support. We acknowledge support by the Medical Core Facilities (Genomics, Flow Cytometry, X-ray, Small Animal Imaging: 7T-MRI and PET-CT). This work was supported by grants from Deutsche Krebshilfe (111250, 70112623 to T. Stiewe and 111444 to O. Timofeev), Deutsche José Carreras Leukämie Stiftung e.V. (09 R/2018 to O. Timofeev and T. Stiewe), Deutsche Forschungsgemeinschaft (TRR81/3 109546710 A10 to T. Stiewe, TI 1028/2-1 to O. Timofeev, STI 182/13-1 to T. Stiewe, DO 545/18-1 to V. Dötsch), German Center for Lung Research (DZL) to T. Stiewe, BMBF (01KX1012 to M. Hrabé de Angelis, 031L0063 to T. Stiewe), and von Behring-Röntgen Stiftung (65-0004 and 66-LV06 to T. Stiewe).

The costs of publication of this article were defrayed in part by the payment of page charges. This article must therefore be hereby marked *advertisement* in accordance with 18 U.S.C. Section 1734 solely to indicate this fact.

Received June 12, 2020; revised July 30, 2020; accepted August 26, 2020; published first September 1, 2020.

References

1. Liu Y, Tavana O, Gu W. p53 modifications: exquisite decorations of the powerful guardian. J Mol Cell Biol 2019;11:564–77.
2. Sykes SM, Mellert HS, Holbert MA, Li K, Marmorstein R, Lane WS, et al. Acetylation of the p53 DNA-binding domain regulates apoptosis induction. Mol Cell 2006;24:841–51.
3. Tang Y, Luo J, Zhang W, Gu W. Tip60-dependent acetylation of p53 modulates the decision between cell-cycle arrest and apoptosis. Mol Cell 2006;24:827–39.
4. Tang Y, Zhao W, Chen Y, Zhao Y, Gu W. Acetylation is indispensable for p53 activation. Cell 2008;133:612–26.
5. Gully CP, Velazquez-Torres G, Shin JH, Fuentes-Mattei E, Wang E, Carlock C, et al. Aurora B kinase phosphorylates and instigates degradation of p53. Proc Natl Acad Sci U S A 2012;109:E1513–22.
6. Wu L, Ma CA, Zhao Y, Jain A. Aurora B interacts with NIR-p53, leading to p53 phosphorylation in its DNA-binding domain and subsequent functional suppression. J Biol Chem 2011;286:2236–44.
7. DeHart CJ, Chahal JS, Flint SJ, Perlman DH. Extensive post-translational modification of active and inactivated forms of endogenous p53. Mol Cell Proteomics 2014;13:1–17.
8. DeHart CJ, Perlman DH, Flint SJ. Impact of the adenoviral E4 Orf3 protein on the activity and posttranslational modification of p53. J Virol 2015;89:3209–20.
9. Riley T, Sontag E, Chen P, Levine A. Transcriptional control of human p53-regulated genes. Nat Rev Mol Cell Biol 2008;9:402–12.
10. Weinberg RL, Veprintsev DB, Fersht AR. Cooperative binding of tetrameric p53 to DNA. J Mol Biol 2004;341:1145–59.
11. Beno I, Rosenthal K, Levitine M, Shaulov L, Haran TE. Sequence-dependent cooperative binding of p53 to DNA targets and its relationship to the structural properties of the DNA targets. Nucleic Acids Res 2011;39:1919–32.
12. Weinberg RL, Veprintsev DB, Bycroft M, Fersht AR. Comparative binding of p53 to its promoter and DNA recognition elements. J Mol Biol 2005;348:589–96.
13. Schlereth K, Beinoraviciute-Kellner R, Zeitlinger MK, Bretz AC, Sauer M, Charles JP, et al. DNA binding cooperativity of p53 modulates the decision between cell-cycle arrest and apoptosis. Mol Cell 2010;38:356–68.
14. Schlereth K, Heyl C, Krampitz AM, Mernberger M, Finkernagel F, Scharfe M, et al. Characterization of the p53 cistrome–DNA binding cooperativity dissects p53′s tumor suppressor functions. PLoS Genet 2013;9:e1003726.
15. Timofeev O, Schlereth K, Wanzel M, Braun A, Nieswandt B, Pagenstecher A, et al. p53 DNA binding cooperativity is essential for apoptosis and tumor suppression *in vivo*. Cell Rep 2013;3:1512–25.
16. Timofeev O, Klimovich B, Schneikert J, Wanzel M, Pavlakis E, Noll J, et al. Residual apoptotic activity of a tumorigenic p53 mutant improves cancer therapy responses. EMBO J 2019;38:e102096.
17. Dehner A, Klein C, Hansen S, Muller L, Buchner J, Schwaiger M, et al. Cooperative binding of p53 to DNA: regulation by protein-protein interactions through a double salt bridge. Angew Chem Int Ed Engl 2005;44:5247–51.
18. Klein C, Planker E, Diercks T, Kessler H, Kunkele KP, Lang K, et al. NMR spectroscopy reveals the solution dimerization interface of p53 core domains bound to their consensus DNA. J Biol Chem 2001;276:49020–7.
19. Kitayner M, Rozenberg H, Kessler N, Rabinovich D, Shaulov L, Haran TE, et al. Structural basis of DNA recognition by p53 tetramers. Mol Cell 2006;22:741–53.
20. Kitayner M, Rozenberg H, Rohs R, Suad O, Rabinovich D, Honig B, et al. Diversity in DNA recognition by p53 revealed by crystal structures with Hoogsteen base pairs. Nat Struct Mol Biol 2010;17:423–9.
21. Kang JG, Lago CU, Lee JE, Park JH, Donnelly MP, Starost MF, et al. A mouse homolog of a human TP53 germline mutation reveals a lipolytic activity of p53. Cell Rep 2020;30:783–92.e5.
22. Leroy B, Anderson M, Soussi T. TP53 mutations in human cancer: database reassessment and prospects for the next decade. Hum Mutat 2014;35:672–88.
23. Adams JM, Harris AW, Pinkert CA, Corcoran LM, Alexander WS, Cory S, et al. The c-myc oncogene driven by immunoglobulin enhancers induces lymphoid malignancy in transgenic mice. Nature 1985;318:533–8.
24. Maddalo D, Manchado E, Concepcion CP, Bonetti C, Vidigal JA, Han YC, et al. *In vivo* engineering of oncogenic chromosomal rearrangements with the CRISPR/Cas9 system. Nature 2014;516:423–7.
25. DuPage M, Dooley AL, Jacks T. Conditional mouse lung cancer models using adenoviral or lentiviral delivery of Cre recombinase. Nat Protoc 2009;4:1064–72.
26. Sperringer JE, Grange RW. *In vitro* assays to determine skeletal muscle physiologic function. Methods Mol Biol 2016;1460:271–91.
27. Hardy D, Besnard A, Latil M, Jouvion G, Briand D, Thepenier C, et al. Comparative study of injury models for studying muscle regeneration in mice. PLoS One 2016;11:e0147198.
28. Gailus-Durner V, Fuchs H, Becker L, Bolle I, Brielmeier M, Calzada-Wack J, et al. Introducing the German Mouse Clinic: open access platform for standardized phenotyping. Nat Methods 2005;2:403–4.
29. Fuchs H, Gailus-Durner V, Adler T, Aguilar-Pimentel JA, Becker L, Calzada-Wack J, et al. Mouse phenotyping. Methods 2011;53:120–35.
30. Rathkolb B, Hans W, Prehn C, Fuchs H, Gailus-Durner V, Aigner B, et al. Clinical chemistry and other laboratory tests on mouse plasma or serum. Curr Protoc Mouse Biol 2013;3:69–100.
31. Holter SM, Garrett L, Einicke J, Sperling B, Dirscherl P, Zimprich A, et al. Assessing cognition in mice. Curr Protoc Mouse Biol 2015;5:331–58.
32. Young L, Sung J, Stacey G, Masters JR. Detection of mycoplasma in cell cultures. Nat Protoc 2010;5:929–34.
33. Matsumura I, Ellington AD. *In vitro* evolution of thermostable p53 variants. Protein Sci 1999;8:731–40.
34. Nikolova PV, Henckel J, Lane DP, Fersht AR. Semirational design of active tumor suppressor p53 DNA binding domain with enhanced stability. Proc Natl Acad Sci U S A 1998;95:14675–80.
35. Chen C, Gorlatova N, Kelman Z, Herzberg O. Structures of p63 DNA binding domain in complexes with half-site and with spacer-containing full response elements. Proc Natl Acad Sci U S A 2011;108:6456–61.
36. Amend SR, Valkenburg KC, Pienta KJ. Murine hind limb long bone dissection and bone marrow isolation. J Vis Exp 2016;14:53936.
37. Gao J, Aksoy BA, Dogrusoz U, Dresdner G, Gross B, Sumer SO, et al. Integrative analysis of complex cancer genomics and clinical profiles using the cBioPortal. Sci Signal 2013;6:pl1.

38. Skinner JJ, Wang S, Lee J, Ong C, Sommese R, Sivaramakrishnan S, et al. Conserved salt-bridge competition triggered by phosphorylation regulates the protein interactome. Proc Natl Acad Sci U S A 2017;114:13453–8.
39. Schlereth K, Charles JP, Bretz AC, Stiewe T. Life or death: p53-induced apoptosis requires DNA binding cooperativity. Cell Cycle 2010;9:4068–76.
40. Parrinello S, Samper E, Krtolica A, Goldstein J, Melov S, Campisi J. Oxygen sensitivity severely limits the replicative lifespan of murine fibroblasts. Nat Cell Biol 2003;5:741–7.
41. Huang J, Yang J, Maity B, Mayuzumi D, Fisher RA. Regulator of G protein signaling 6 mediates doxorubicin-induced ATM and p53 activation by a reactive oxygen species-dependent mechanism. Cancer Res 2011;71:6310–9.
42. Demaria M, O'Leary MN, Chang J, Shao L, Liu S, Alimirah F, et al. Cellular senescence promotes adverse effects of chemotherapy and cancer relapse. Cancer Discov 2017;7:165–76.
43. Chambers SM, Shaw CA, Gatza C, Fisk CJ, Donehower LA, Goodell MA. Aging hematopoietic stem cells decline in function and exhibit epigenetic dysregulation. PLoS Biol 2007;5:e201.
44. Tyner SD, Venkatachalam S, Choi J, Jones S, Ghebranious N, Igelmann H, et al. p53 mutant mice that display early ageing-associated phenotypes. Nature 2002; 415:45–53.
45. Maier B, Gluba W, Bernier B, Turner T, Mohammad K, Guise T, et al. Modulation of mammalian life span by the short isoform of p53. Genes Dev 2004;18:306–19.
46. Liu D, Ou L, Clemenson GD Jr, Chao C, Lutske ME, Zambetti GP, et al. Puma is required for p53-induced depletion of adult stem cells. Nat Cell Biol 2010;12: 993–8.
47. Zhao Y, Wu L, Yue X, Zhang C, Wang J, Li J, et al. A polymorphism in the tumor suppressor p53 affects aging and longevity in mouse models. Elife 2018;7:e34701.
48. Eischen CM, Weber JD, Roussel MF, Sherr CJ, Cleveland JL. Disruption of the ARF-Mdm2-p53 tumor suppressor pathway in Myc-induced lymphomagenesis. Genes Dev 1999;13:2658–69.
49. Christopoulos P, Dietz S, Kirchner M, Volckmar AL, Endris V, Neumann O, et al. Detection of TP53 mutations in tissue or liquid rebiopsies at progression identifies ALK+ lung cancer patients with poor survival. Cancers 2019;11:124.
50. Kron A, Alidousty C, Scheffler M, Merkelbach-Bruse S, Seidel D, Riedel R, et al. Impact of TP53 mutation status on systemic treatment outcome in ALK-rearranged non-small-cell lung cancer. Ann Oncol 2018:29:2068–75.
51. Hsu JM, Chen CT, Chou CK, Kuo HP, Li LY, Lin CY, et al. Crosstalk between Arg 1175 methylation and Tyr 1173 phosphorylation negatively modulates EGFR-mediated ERK activation. Nat Cell Biol 2011;13:174–81.
52. Albrecht LV, Ploper D, Tejeda-Munoz N, De Robertis EM. Arginine methylation is required for canonical Wnt signaling and endolysosomal trafficking. Proc Natl Acad Sci U S A 2018;115:E5317–25.
53. Kim S, Kim NH, Park JE, Hwang JW, Myung N, Hwang KT, et al. PRMT6-mediated H3R2me2a guides Aurora B to chromosome arms for proper chromosome segregation. Nat Commun 2020;11:612.
54. Andreeff M, Kelly KR, Yee K, Assouline S, Strair R, Popplewell L, et al. Results of the phase I trial of RG7112, a small-molecule MDM2 antagonist in leukemia. Clin Cancer Res 2016;22:868–76.
55. Abbas HA, Maccio DR, Coskun S, Jackson JG, Hazen AL, Sills TM, et al. Mdm2 is required for survival of hematopoietic stem cells/progenitors via dampening of ROS-induced p53 activity. Cell Stem Cell 2010;7:606–17.
56. Ringshausen I, O'Shea CC, Finch AJ, Swigart LB, Evan GI. Mdm2 is critically and continuously required to suppress lethal p53 activity *in vivo*. Cancer Cell 2006;10: 501–14.
57. Mendrysa SM, O'Leary KA, McElwee MK, Michalowski J, Eisenman RN, Powell DA, et al. Tumor suppression and normal aging in mice with constitutively high p53 activity. Genes Dev 2006;20:16–21.
58. Terzian T, Wang Y, Van Pelt CS, Box NF, Travis EL, Lozano G. Haploinsufficiency of Mdm2 and Mdm4 in tumorigenesis and development. Mol Cell Biol 2007;27:5479–85.
59. Garcia-Cao I, Garcia-Cao M, Martin-Caballero J, Criado LM, Klatt P, Flores JM, et al. "Super p53" mice exhibit enhanced DNA damage response, are tumor resistant and age normally. EMBO J 2002;21:6225–35.
60. Bondar T, Medzhitov R. p53-mediated hematopoietic stem and progenitor cell competition. Cell Stem Cell 2010;6:309–22.
61. Jaiswal S, Ebert BL. Clonal hematopoiesis in human aging and disease. Science 2019;366:eaan4673.
62. Katayama H, Sasai K, Kawai H, Yuan ZM, Bondaruk J, Suzuki F, et al. Phosphorylation by aurora kinase A induces Mdm2-mediated destabilization and inhibition of p53. Nat Genet 2004;36:55–62.
63. Liu Q, Kaneko S, Yang L, Feldman RI, Nicosia SV, Chen J, et al. Aurora-A abrogation of p53 DNA binding and transactivation activity by phosphorylation of serine 215. J Biol Chem 2004;279:52175–82.
64. Vilgelm AE, Pawlikowski JS, Liu Y, Hawkins OE, Davis TA, Smith J, et al. Mdm2 and aurora kinase a inhibitors synergize to block melanoma growth by driving apoptosis and immune clearance of tumor cells. Cancer Res 2015;75: 181–93.
65. Lee DF, Su J, Ang YS, Carvajal-Vergara X, Mulero-Navarro S, Pereira CF, et al. Regulation of embryonic and induced pluripotency by aurora kinase-p53 signaling. Cell Stem Cell 2012;11:179–94.

Cancer Research
The Journal of Cancer Research (1916–1930) | The American Journal of Cancer (1931–1940)

AACR American Association for Cancer Research

Phosphorylation Control of p53 DNA-Binding Cooperativity Balances Tumorigenesis and Aging

Oleg Timofeev, Lukas Koch, Constantin Niederau, et al.

Cancer Res 2020;80:5231-5244. Published OnlineFirst September 1, 2020.